substance: CeH_x
property: crystal structure, physical properties

crystal structure		cubic (O_h^5 – Fm3m)		72L1, 72L2
lattice parameter				
a	5.539 Å	x = 3		66H
electrical conductivity				
σ	≈ 10 Ω^{-1} cm^{-1}	x = 2.81, n-type		69L
	≈ 3 Ω^{-1} cm^{-1}	x = 2.85		69L, 72L1
activation energy for conductivity				
E_A	0.104 eV	x = 2.81, T = 200 K		72L2
CeH_{2+x} [95V]				
semiconductor:	x = 0.70		M-SC transition: T = 260(10) K (heating)	88S
ρ	5500 μΩcm	T = 260 K		
semiconductor:	x = 0.78		M-SC transition: T = 230(10) K (heating)	88S
ρ	2400 μΩcm	T = 230 K		
semiconductor:	x = 0.715		M-SC transition: T = 245(5) K (cooling)	72L1
ρ	$1\cdot10^4$ μΩcm	T = 245 K		
semiconductor:	x = 0.74		M-SC transition: T = 200(10) K (cooling)	72L1
ρ	$1.7\cdot10^4$ μΩcm	T = 200 K		
semiconductor:	x = 0.77		M-SC transition: T = 220(5) K (cooling)	72L1
ρ	$2.3\cdot10^4$ μΩcm	T = 220 K		
			normalized resistivity vs. T: Fig. 3,	
			XPS-spectrum: Fig. 1, UPS-spectrum: Fig. 2	

Further figures and references:

crystal structure: Fig. 4

lattice parameter vs. x: Fig. 6

metal-semiconductor transition for x ≥ 2.7 [72L1, 79D, 81F1]

heat capacity [65B]; temperature dependence of heat capacity (x = 2.7, 2.96): Fig. 5

energy bands (x = 3): Fig. 7

density of states (x = 3, 2.75): Figs. 8, 9

XPS spectra (x = 2.9): Figs. 10, 11

Hall coefficient: Fig. 12

charge carrier concentration: Fig. 13

Seebeck coefficient: Fig. 14

resistivity dependence on x: Fig. 15; temperature dependence of resistivity for x = 2.77, 2.81, 2.85: Figs. 16, 17, 18

optical phonon energies 110 meV and 65 meV for x = 2.72 [74V];

electron phonon interaction [81F2]

References:

65B Biegatiski, Z., Fesenko, W., Stalinski, B.: Bull. Acad. Pol. Sci., Ser. Sci. Chim. 3 (1965) 227.

66H Hardeastle, K. I., Warf, J. C.: Inorg. Chem. 5 (1966) 1728.

68M Mueller, W. M., in: Metal Hydrides, Mueller, W. M., Blackledge, J. P., Libowitz, G. G. (eds.), N. Y.: Academic Press, 1968, p. 384.

69H Heckman, R. C.: Electronic Properties of Rare Earth Hydrides, Report No. SC-RR-69-571, Sandia Laboratories, Albuquerque, N. M., Nov. 1969.

69L Libowitz, G. G., Pack, J. G.: J. Chem. Phys. 50 (1969) 3557.

72L1 Libowitz, G. G.: Ber. Bunsenges. Phys. Chem. 8 (1972) 837.

72L2 Libowitz, G. G., Pack, J. G., Binnie, W. P.: Phys. Rev. B 6 (1972) 4540.

74V Vorderwisch, P., Hautecler, S.: Phys. Stat. Solidi (b) 64 (1964) 495.

79B Bieganski, Z., Stalinski, B.: Z. Phys. Chem. Neue Folge 116 (1979) 109.

79D Drulis, M., Bieganski, Z.: Phys. Status Solidi (a) 53 (1979) 277.

80F Fujimori, A., Minami, F., Tsuda, N.: Phys. Rev. B 22 (1980) 3573.

81F1 Fujimori, A., Tsuda, N.: J. Phys. C 14 (1981) 1427.

81F2 Fujimori, A., Tsuda, N.: J. Phys. C 14 (1981) L69.

82S Schlapbach, L., Osterwalder, J.: Solid State Commun. 42 (1982) 271.

85O Osterwalder, J: Z. Phys. B 61 (1985) 113.

87S Schlapbach, L., Burger, J.P., Bonnet, J.E., Thiry, P., Petroff, Y.: Surf. Sci. 189/190 (1987) 747.

88S Shinar, J., Dehner, B., Beaudry, B.J., Peterson, D.T.: Phys. Rev. B 37 (1988) 2066.

89S Shinar, J., Dehner, B., Beaudry, B.J.: Z. Phys. Chem. NF 163 (1989) 591.

95V Vajda, P.: "Hydrogen in rare-earth metals, including RH_{2+x} Phases" in: Handbook on the Physics and Chemistry of Rare Earth, Vol. 20, Gschneidner, K.A., Jr., Eyring, L. (eds.), Elsevier Science, 1995, p. 207.

Fig. 1.

RH_x. Valence band spectra for La, Y, Ce, and Pr and for their phase boundary and trihydride compositions from XPS. Data for the metals are shown by dotted lines [85O].

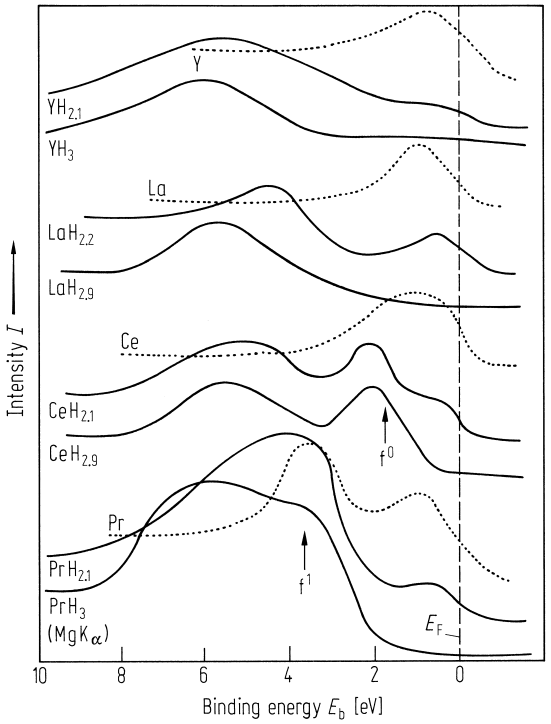

Fig. 2.

RH_x. UPS photoemission data for hydrides of La, Ce, Gd, and Tb at binding energies near the Fermi level [87S].

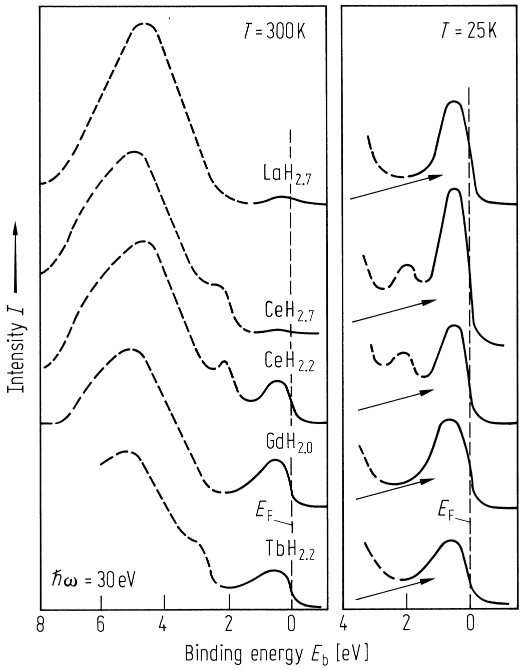

Fig. 3.

CeH_{2+x}. Normalized resistivity $\rho(T)/\rho(295K)$ as a function of the (inverse) temperature, showing metal-semiconductor transitions and pure semiconductor behaviour. The actual H content of the $CeH_{2.81}$ sample was probably somewhat higher than indicated [89S].

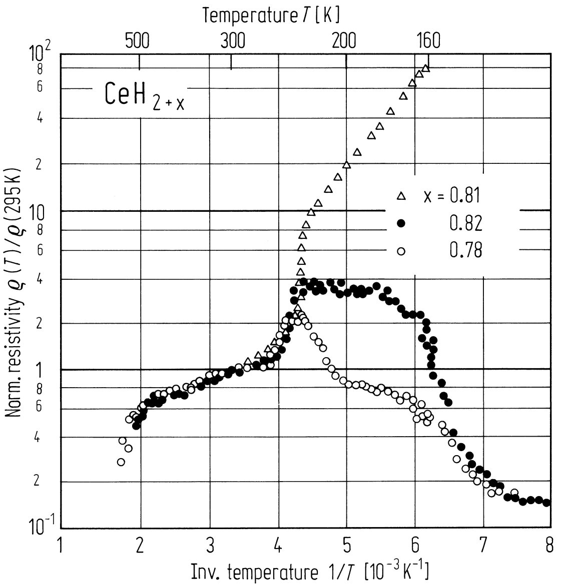

Fig. 4.

REH_x. Unit cell of the CaF_2-type structure.

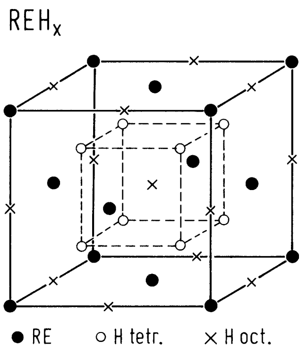

Fig. 5.

RH_x, R = La, Ce, Pr, Nd, Sm. Molar heat capacities vs. temperature. The maxima at about 250 K are attributed to metal-semiconductor transitions. No anomaly was found for $CeH_{2.96}$ and $SmH_{2.84}$ in this temperature range [79B].

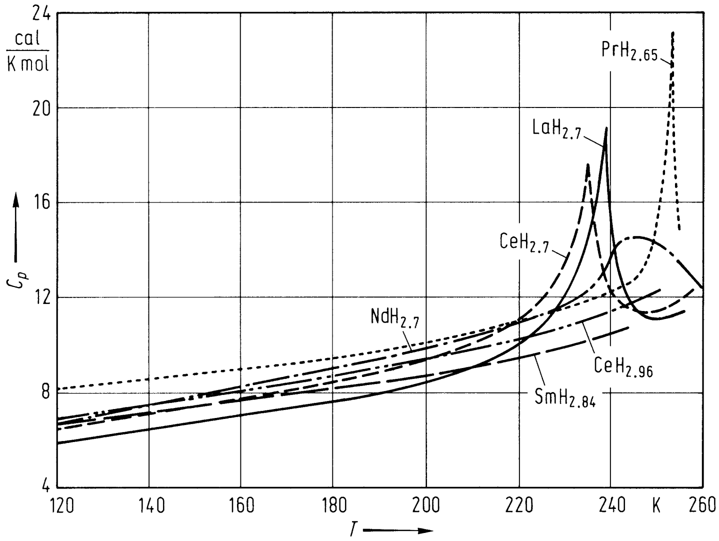

Fig. 6.

CeH_x. Lattice parameter as a function of hydrogen concentration [68M].

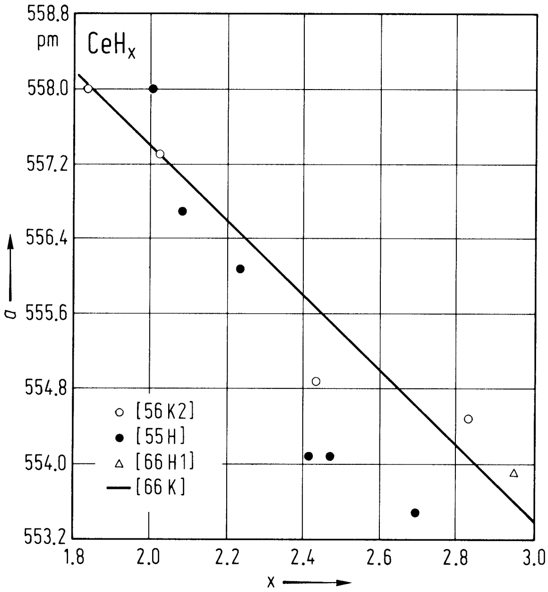

Fig. 7.

CeH_3. Energy bands obtained from an APW calculation [80F].

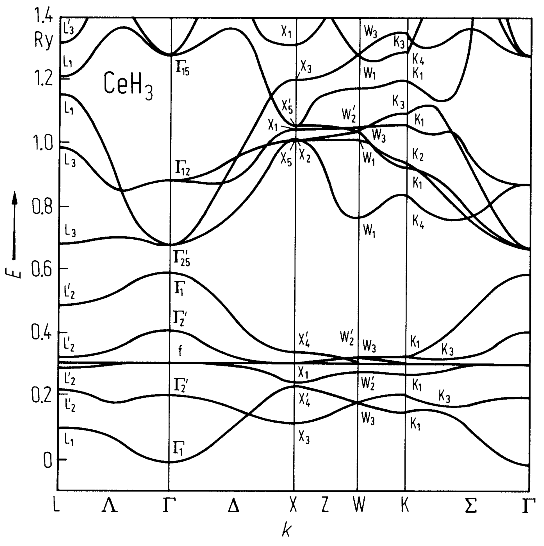

Fig. 8.

CeH_3. Partial and total density of states [80F]. H_{oct}, H_{tetr}: octahedral and tetrahedral H, respectively.

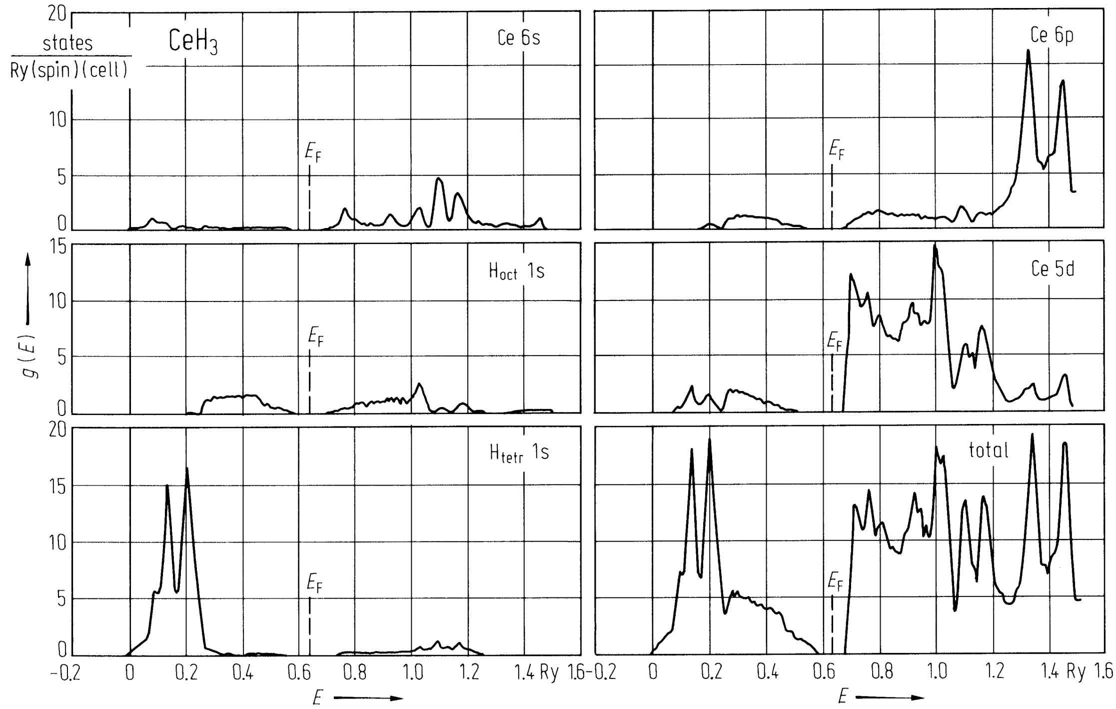

Fig. 9.

$CeH_{2.75}$. Density of states for bct and cubic supercells [81F1].

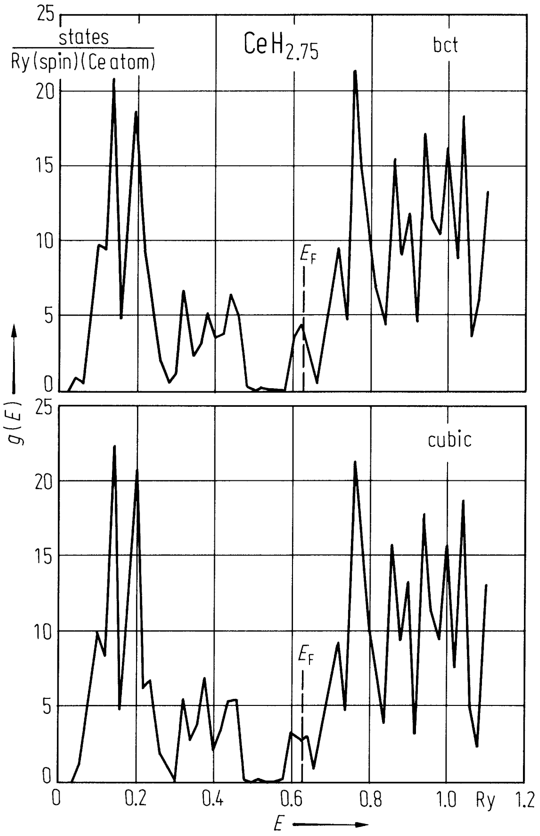

Fig. 10.

$CeH_{2.9}$, Ce. XPS-spectra (intensity vs. binding energy). A comparison of 3d core level spectra [82S].

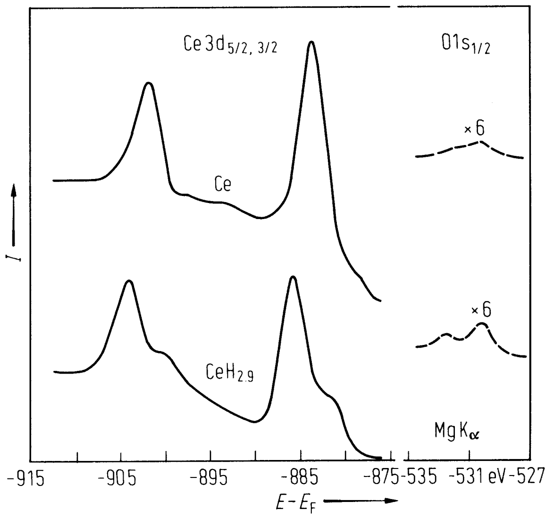

Fig. 11.

$CeH_{2.9}$, Ce. XPS valence band and 5p core level spectra (intensity vs. binding energy) [82S].

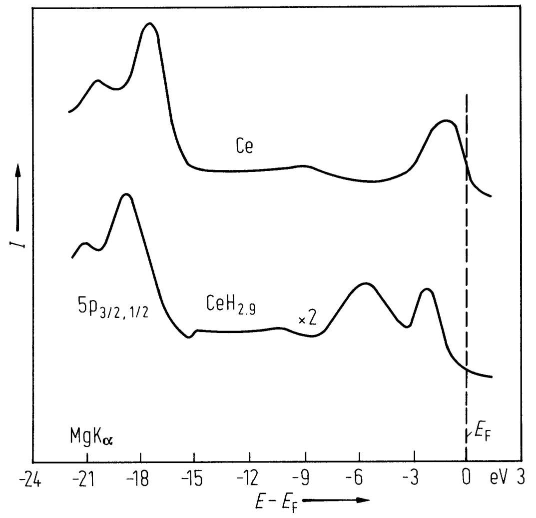

Fig. 12.

CeH_x. Hall coefficient vs. composition in the rang $2.0 \le x \le 2.8$ [69H].

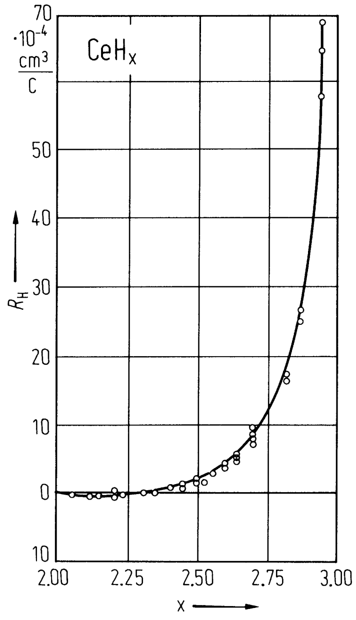

Fig. 13.

CeH_x. Charge carrier concentration vs. composition for 2.3 ≤ x ≤ 2.8. The straight line is predicted for the case of one hole removed for each hydrogen added [69H].

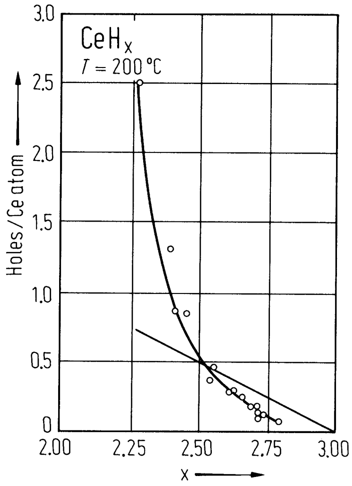

Fig. 14.

CeH_x. Seebeck coefficient vs. temperature for several compositions [72L1].

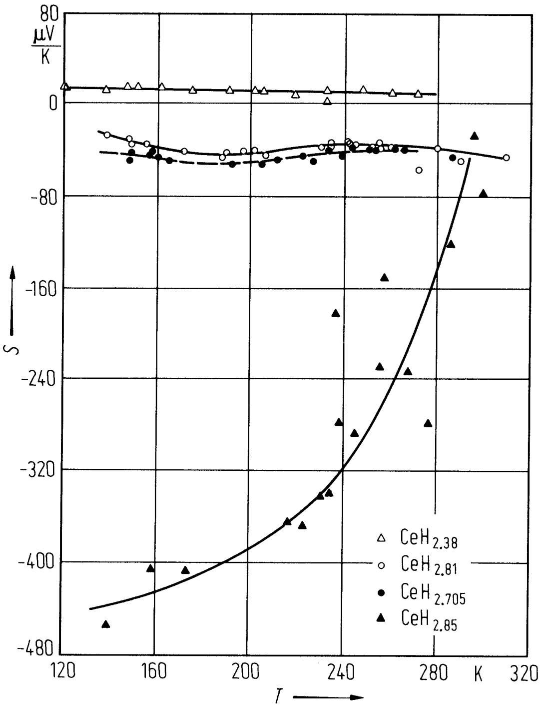

Fig. 15.

CeH_x. Resistivity vs. composition. Measurements by various authors [72L1].

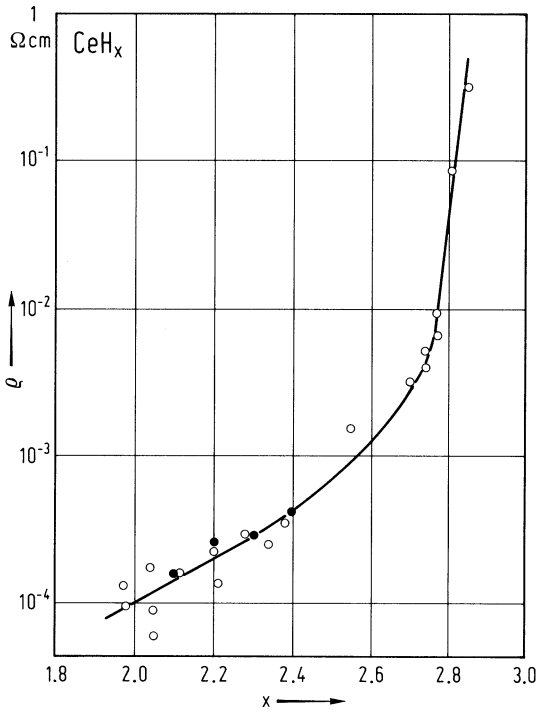

Fig. 16.

$CeH_{2.77}$. Resistivity vs temperature [72L1].

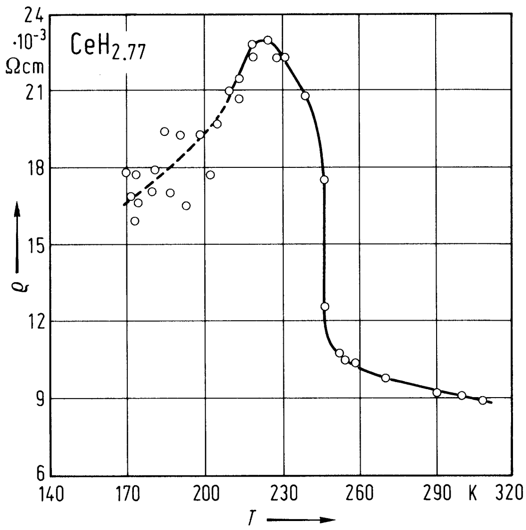

Fig. 17.

$CeH_{2.81}$. Resistivity vs. reciprocal temperature [72L2].

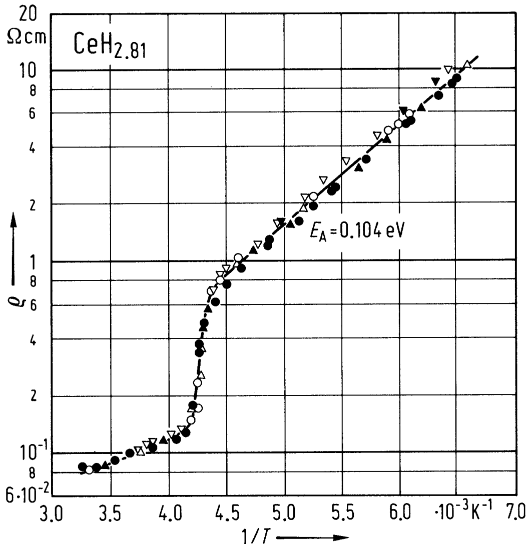

Fig. 18.

$CeH_{2.85}$. Resistivity vs. (reciprocal) temperature [69L, 72L1].